Topological surface state under graphene for two-dimensional spintronics in air

A. Varykhalov[1], D. Marchenko[1], M. R. Scholz[1], E. Rienks[1], T. K. Kim[2], O. Rader[1]
[1] *Helmholtz-Zentrum Berlin für Materialien und Energie, Elektronenspeicherring BESSY II, Albert-Einstein-Str. 15, D-12489 Berlin, Germany and*
[2] *Institute for Solid State Research, IFW Dresden, P.O. Box 270116, D-01171 Dresden, Germany*

Spin currents which allow for a dissipationless transport of information can be generated by electric fields in semiconductor heterostructures in the presence of a Rashba-type spin-orbit coupling. The largest Rashba effects occur for electronic surface states of metals but these cannot exist but under ultrahigh vacuum conditions. Here, we reveal a giant Rashba effect ($\alpha_R \approx 1.5 \cdot 10^{-10}$ eVm) on a surface state of Ir(111). We demonstrate that its spin splitting and spin polarization remain unaffected when Ir is covered with graphene. The graphene protection is, in turn, sufficient for the spin-split surface state to survive in ambient atmosphere. We discuss this result along with evidences for a topological protection of the surface state.

The Rashba effect in spintronics is based on symmetry breaking [1]: In the bulk of crystallographically inversion symmetric solids the time reversal symmetry results in degenerate spin subbands of electronic valence states. At crystal surfaces or interfaces this structural inversion symmetry is broken and spin degeneracy is lifted. A gradient of the electric field perpendicular to the surface will then lead to a Rashba effect in two-dimensional systems with large spin-orbit coupling [2]. It emerges as a splitting of the band structure into subbands $E_{\pm}(\mathbf{k}_{\parallel})$ of opposite spin which are displaced by electron wave vectors $\pm\Delta\mathbf{k}_{\parallel}$ in opposite directions in momentum space. Regarding the transport properties of the solid and their applications, this leads to the generation of dissipationless spin currents without the necessity for ferromagnetic materials or magnetic fields [3, 4].

In the quantum mechanical description of a two-dimensionally confined electron gas, the Rashba effect is accounted for by the Hamiltonian

$$H_R = \alpha_R \left(\sigma_x \frac{\partial}{\partial y} - \sigma_y \frac{\partial}{\partial x} \right)$$

where σ denotes Pauli spin matrices and the parameter α_R is proportional to the potential gradient ∇V in z-direction and accounts for the size of the spin-orbit interaction. For free electrons, the two spin-split bands $E_{\pm}(\mathbf{k}_{\parallel})$ are described by

$$E_{\pm}(\mathbf{k}_{\parallel}) = \frac{\hbar^2 {\mathbf{k}_{\parallel}}^2}{2m^*} \pm \alpha_R |\mathbf{k}_{\parallel}|,$$

where m^* is the effective mass. The two $E_{\pm}(\mathbf{k}_{\parallel})$ parabolas are shifted relative to the origin $\overline{\Gamma}$ ($\mathbf{k}_{\parallel} = 0$) by a momentum splitting $\Delta\mathbf{k}_{\parallel} = (m^*\alpha_R)/\hbar^2$.

The Rashba effect has been investigated first and foremost for semiconductor heterostructures [2], reaching Rashba parameters of up to $4 \cdot 10^{-11}$ eVm in InAs-based structures [6]. It has been shown that a Rashba-split system leads to an intrinsic spin Hall effect [3, 4]. An electric field applied along in the two-dimensional interface plane leads during charge transport to a tilting of the spins in opposite directions depending on the propagation direction [3–5]. Spintronics does not require semiconducting materials because it does not depend on charge currents and their amplification. Spin currents produced by the spin Hall effect in all-metal devices are much larger than in semiconductors [7, 8]. Also, the largest Rashba effects have been measured for metal surface states which are localized at the outermost atomic layers of the solid-vacuum interface. Discovered by Russian theoretician Igor Tamm in 1932 [9], metal surface states had to wait for their experimental scrutiny until ultrahigh vacuum sample environments became available [10]. They are highly sensitive to adsorbates, and it is hard to conceive an adsorbate that will leave a surface state unaffected while protecing it against the influence of air.

The most prominent example of the Rashba effect at metal surfaces is the L-gap surface state on Au(111) [11, 12]. Spin- and angle-resolved photoelectron spectroscopy reveals a large spin-orbit splitting ($\alpha_R = 3.3 \cdot 10^{-11}$ eVm) [11]. Rashba-type splittings were also evidenced in Bi [13] and W(110) covered by monolayers of hydrogen [14], Li [15] Au, and Ag [16]. Large spin-orbit effects were recently observed in quantum well states of Au/W(110) ($\alpha_R \approx 1.6 \cdot 10^{-11}$ eVm) [17] and also Pb/Si(111) ($\alpha_R \approx 4 \cdot 10^{-12}$ eVm) [18]. A Rashba effect emerges also in the linear bands of massless Dirac fermions in graphene on a Au monolayer [19]. The term *giant Rashba effect* has been coined recently for a Rashba parameter α_R of the order of 10^{-10} eVm for a surface state of Bi/Ag(111) ($\alpha_R \approx 4$–$6 \cdot 10^{-10}$ eVm) [20]. For all these states holds that they cannot exist but in ultrahigh vacuum and, therefore, have no apparent practical application.

Figures 1 and 2 show the characterization of clean and graphene-covered Ir samples. Bare Ir(111) shows a sharp $p(1 \times 1)$ pattern in low-energy electron diffraction (LEED). The LEED image of graphene/Ir(111) (Fig. 1b) reveals a characteristic diffraction pattern with multiple satellite spots which are due to the formation of a superstructure of the moiré type which, in turn, is

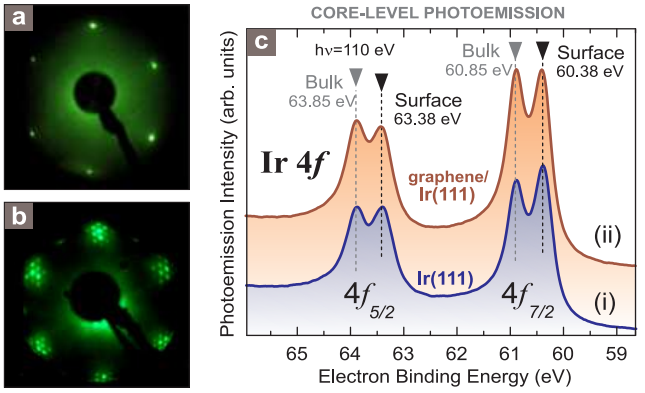

Figure 1. Preparation of epitaxial graphene.(**a**) LEED image of bare Ir(111) and (**b**) of moiré-patterned graphene/Ir(111). (**c**) Comparison of $4f$ core-level spectra measured from (i) bare Ir(111) and (ii) graphene/Ir(111). The surface component remains unchanged.

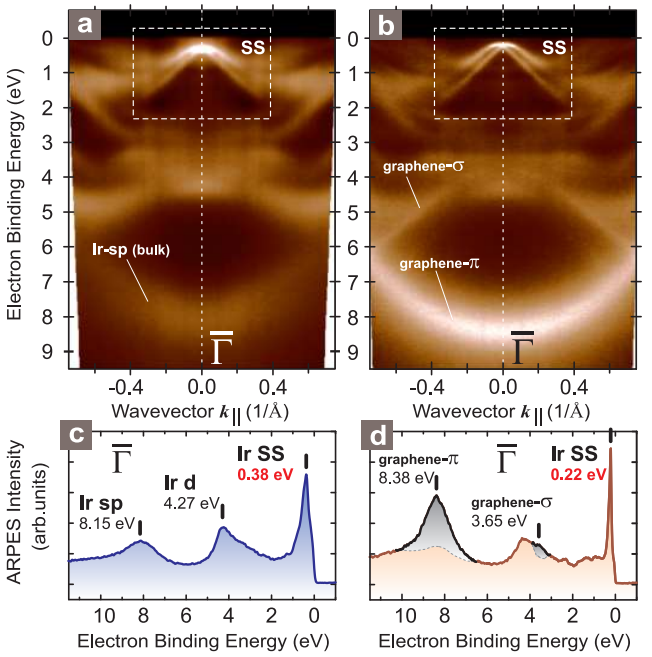

Figure 2. Overall valence band structure. (**a**) Bare Ir(111) and (**b**) graphene-covered Ir(111) ($h\nu = 62$ eV). Spin-orbit split surface state (SS) is marked with a white frame. (**c, d**) normal-emission spectra [corresponding to the $\overline{\Gamma}$-point of the surface Brillouin zone] extracted from (**a**) and (**b**), respectively. The spectra allow for a quantitative comparison between intensities of Ir surface state and graphene bands.

caused by a large misfit (∼10%) between crystal lattices of graphene and Ir [21]. The high structural quality of the moiré-patterned graphene is also confirmed by direct microscopic characterization with scanning tunneling microscopy [5].

Figure 1c shows the Ir $4f_{5/2}$ and $4f_{7/2}$ core levels, both with components originating from inside the bulk and from the surface. The components at 0.5 eV lower binding energy are exclusively due to emission from the topmost atomic layer of Ir(111) [22], and they were shown by oxygen adsorption to be very sensitive to the local atomic environment [23]. It is, therefore, remarkable that the spectra of the Ir$4f$ core level in Fig. 1c *cannot* be used as indicator for the presence of graphene on Ir(111). On the contrary, the formation of graphene on top does not visibly affect the surface component and line fits show that the energy splitting between bulk and surface components decreases by only 2% [24]. This indicates very weak graphene-Ir interaction and is in line with the observation that Ir(111) is a metal substrate that supports the formation of an ideal quasifreestanding electronic structure of graphene [27], similar to the substrate Au/Ni(111) [19].

Figs. 2a and 2b compare the overall valence band structure of Ir(111) before and after formation of graphene, respectively. For graphene/Ir(111) (Fig. 2b) one can see strongly dispersing graphene-derived π- and σ-states reaching at $\overline{\Gamma}$ binding energies of 8.38 eV and 3.65 eV, respectively. (Note that the π- and σ-dispersions are accidentally degenerate with emission from Ir bulk bands.) The high structural quality of the synthesized graphene is additionally confirmed by the observation of a sharp conical dispersion of Dirac fermions at the $\overline{\text{K}}$-point [5].

The comparison between Figures 2a and 2b delivers another important message: Apparently, the Ir bands preserve their overall dispersions and binding energies upon graphene deposition. This agrees well with the weak interaction between graphene and Ir(111), noted above. In this context, very intriguing is the band showing up at 0.2–0.3 eV below E_F at $\overline{\Gamma}$ [the region is marked by a frame and the dispersion is denoted as SS in Figs. 2a and 2b]. From studies at $\overline{\Gamma}$ this band is known to be an Ir(111) surface state situated at 0.4 eV binding energy above the bulk L_{6-} point at 1 eV binding energy [25]. The state is related to the L-gap surface states of Au(111) but in Ir the bulk bands have a different order so that the surface state is reversed (i. e., with effective mass $m^* < 0$). It is seen now that this surface state is also clearly split in $\mathbf{k}_\parallel$, resembling classical Rashba-type spin-orbit split surface states [11]. The splitting amounts to $2\Delta\mathbf{k}_\parallel = 0.075$ Å^{-1}. The population of this state remains unaffected by the formation of graphene on Ir(111). This can be seen quantitatively in normal-emission ($\overline{\Gamma}$) spectra plotted in Figs. 2c and 2d. We paid attention explicitly to the splitting sampling the surface-state region with enhanced angular and energy resolution. The dispersion acquired for bare Ir(111) is shown in Fig. 3a. Indeed, the electronic state is composed of two identical parabolic bands shifted by ±0.04 Å^{-1} relative to $\overline{\Gamma}$. The binding energy of the top of the bands is determined as 340 meV. Fig. 3b demonstrates what happens to the split-state when graphene

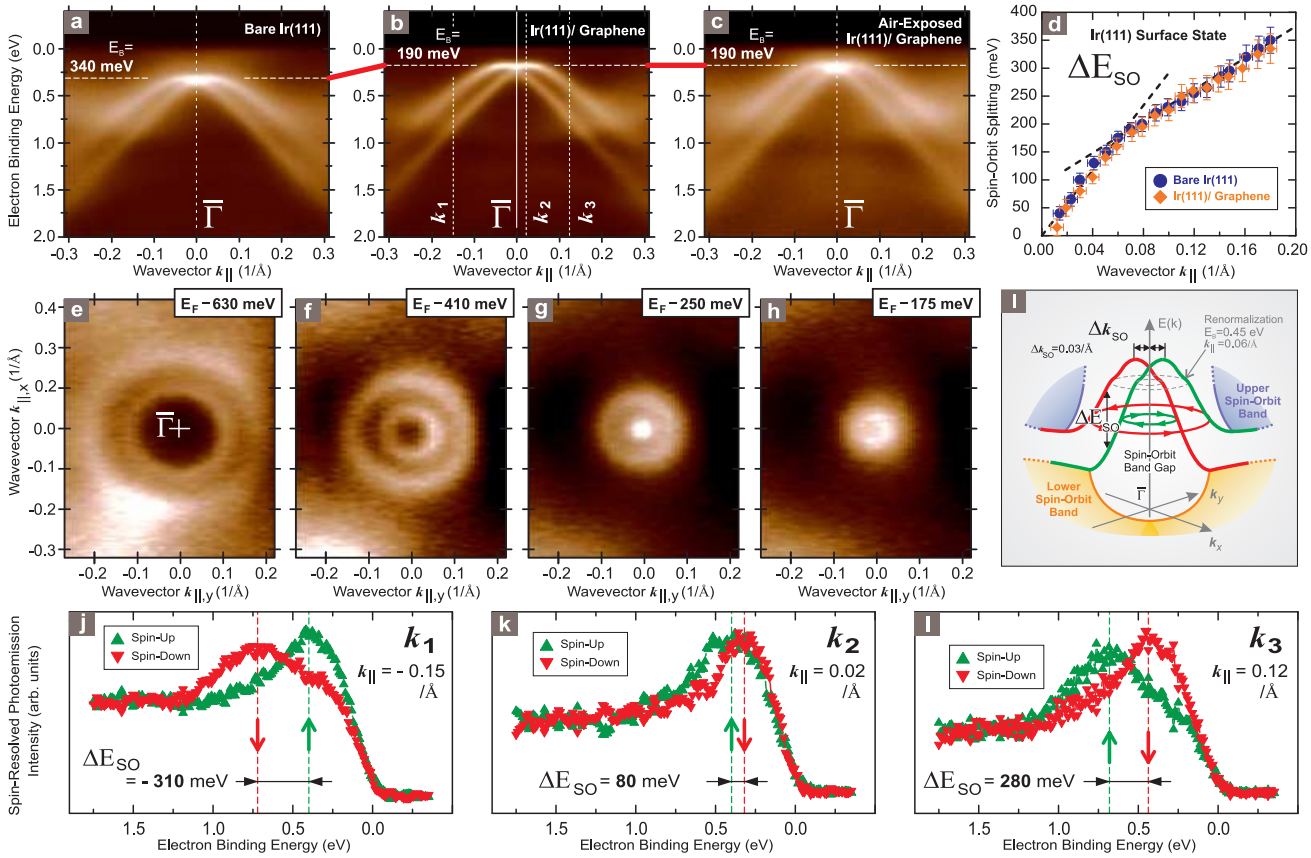

Figure 3. Characterization of the spin-orbit split surface state on Ir(111). Dispersion of surface state on (**a**) bare Ir(111) and (**b**) under graphene grown on Ir(111). (**c**) Dispersion of surface state under graphene on Ir(111) after exposure to ambient atmosphere for 15 min. (**d**) Detailed comparison of spin-orbit splitting $\Delta E_{SO}(k_{\|})$ for bare and graphene-covered Ir(111). (**e**–**h**) Constant energy surfaces of the Ir surface state extracted from full-photoemission mapping around $\overline{\Gamma}$. In agreement with the Rashba model, two circles are revealed corresponding to opposite directions of spin circulation. (**i**) Sketch of spin-orbit splitting and spin-topology of the surface state indicating topological protection. (**j**–**l**) Direct proof of spin-splitting in Ir surface state under graphene by spin-resolved photoemission. Measured spectra correspond to wave-vectors k_1, k_2 and k_3 as denoted in (**b**). The photon energy was 62 eV.

is grown on top: The only change concerns the binding energy of the parabolic bands, which decreases by 150 meV to 190 meV. (The different sharpness of the bands is not a systematic effect.) This is clear evidence that the split band is a *surface state* of Ir(111) which persists *under* graphene.

Results of a full photoemission mapping of the Ir surface state under graphene are presented in Figs. 3(e-h) as a sequence of constant energy surfaces cut at binding energies of 630, 410, 250 and 175 meV. The maps are fully consistent with the Rashba mechanism of spin-orbit splitting: For higher binding energies two circles are observed which correspond to opposite directions of spin circulation (arrowheads in Fig. 3i). At ∼250 meV, the inner circle shrinks to a point which is the Kramers point of spin degeneracy, and for 175 meV binding energy only one circle is left, which corresponds to the only direction of spin rotation. This mapping also shows that two bands that disperse in parallel from the zone centre as have been obtained from Ir(111) recently [26] can easily result from a slight misalignment of the experimental setup.

We have additionally confirmed this Rashba scenario through direct observation of the spin. Spin-resolved spectra measured for the emission angles corresponding to the electron wave vectors k_1, k_2 and k_3 [labels of Fig. 3c] are displayed in Figs. 3j–l. Indeed, the splitting of the bands is a spin splitting. The splitting ΔE_{SO} is large for $k_3 > 0$ far from $\overline{\Gamma}$, decreases for k_2 closer to $\overline{\Gamma}$, and, expectedly, reverses for $k_1 < 0$.

We have fitted the surface-state dispersions shown in Figs. 3a and 3b and investigated how the spin-orbit splitting ΔE_{SO} behaves with wave-vector $k_{\|}$ for bare Ir(111) and for graphene-covered Ir(111). Fig. 3d shows that in both cases $\Delta E_{SO}(k_{\|})$ is linear, corresponding to parabolic, free-electron-like bands, and fulfills the criterion $\Delta E_{SO}(k_{\|} = 0) = 0$ of the Rashba effect. However, ΔE_{SO} suffers a kink at $k_{\|}$=0.06 Å^{-1}. This can be as-

cribed to the interaction of the surface state with Ir bulk d-bands in this range because the surface states are partially degenerate with bulk bands [25] and, are therefore rather surface resonances.

The other surprising information available from Fig. 3d is a *quantitative* equality of the Rashba splitting ΔE_{SO} for bare Ir(111) and for graphene/Ir(111). According to a recent analysis [28] there is a large and universal charge gradient ΔV at any graphene-metal interface which can be estimated for graphene/Ir(111) from the work functions of Ir(111), 5.8 eV, and of graphene, 4.5 eV, and the Fermi-energy shift ΔE_{F}, 0.1 eV, as 1.2 eV. The surface potential has been assigned an important role for the Rashba effect [12, 14, 15]. Based on Li/W(110) adsorption experiments, the spin-orbit splitting has even been suggested as local probe of surface potential gradients [15]. Previously, we found no such influence for Au/W(110) and related systems [17]. Here, the change in surface potential modifies the binding energy but not the spin-orbit splitting of the present surface state. The spin-orbit effect is therefore assigned to the large potential gradient of nuclear charge of the ^{77}Ir atoms.

Before closing, we want to address the reason for the robustness of the surface state. Recently, topological surface states have been predicted and observed which are spin-orbit split and protected by time-reversal symmetry [29–31], and it is the question whether the presently encountered stability of the surface state towards graphene deposition is related. It was pointed out recently [30] that the spin-polarized and Rashba-split L-gap surface state of Au(111) does not fulfil the criterion for topological protection, which is an odd number of Fermi level crossings between two time-reversal invariant k-points of the surface Brillouin zone, as occurs with the surface state identified on Bi_2Se_3 [30]. Unlike on Au, the present Ir surface state becomes degenerate with bulk d-bands, and its tails connect to bulk d bands as seen in Fig 2. We can demonstrate experimentally that this state connects L_{6-} and L_{6+} bulk states of Ir.[5] While it apparently does not fulfil the criterion for topological insulators of an odd number of crossings of E_{F} between the two time-reversal invariant $\mathbf{k}$-points $\overline{\Gamma}$ and $\overline{\mathrm{M}}$, this criterion, if adopted to the metal Ir, has to consider instead of the Fermi level a curved line lying between these bulk bands, and such line is crossed by the surface state in fact only an odd number of times between $\overline{\Gamma}$ and $\overline{\mathrm{M}}$.[5] A similar situation has been found for the (111) surface of Sb recently. [31]

Finally, considering the ability of the spin-split surface state to exist under graphene, we have tested how well graphene may protect the Ir surface state from the environment. We have exposed a graphene-covered Ir(111) sample to ambient atmosphere for 15 min and measured the dispersion of the surface state right after this. The result is presented in Fig. 3c. Although a somewhat stronger background is seen due to remaining adsorbates, an accurate analysis shows that neither binding energy nor spin splitting of the surface state are influenced by the air (Fig. 3d). In a technological context this means that graphene, weakly interacting with its substrate, can be considered an ideal capping layer, which on the one hand protects metallic surfaces from a chemically reactive environment [32], and on the other hand keeps its electronic and spin structure intact even at the atomic level of surface electronic states which are most promising generators of two-dimensional spin currents.

In summary, we have demonstrated (i) a previously unknown Rashba-type splitting of giant size of a surface state on Ir(111), (ii) that the surface state survives when Ir(111) becomes covered with epitaxial graphene while it changes its binding energy by 150 meV, (iii) that neither dispersion nor Rashba splitting of the surface state are influenced by the presence of graphene on top of Ir(111), (iv) that the spin-dependent band dispersion is consistent with topological protection, (v) and that graphene protects the surface electronic structure of Ir(111) so well that the spin-orbit split surface state survives the exposure of the sample to ambient atmosphere.

Methods

For information on experimental methods and sample characterization please see the Supplementary Information [33].

[1] E. I. Rashba, Fiz. Tver. Tela (Leningrad) 2, 1224 (1960), [Properties of semiconductors with an extremum loop. 1. Cyclotron and combinational resonance in a magnetic field perpendicular to the plane of the loop, Sov. Phys. Solid State 2, 1109 (1960)]; Y. A. Bychkov and E. I. Rashba, Oscillatory effects and the magnetic susceptibility of carriers in inversion layers, J. Phys. C 17, 6039 (1984).

[2] R. Winkler, Spin-Orbit Coupling Effects in Two-Dimensional Electron and Hole Systems, Springer, Berlin (2003).

[3] S. Murakami, N. Nagaosa, and S.-C. Zhang, Dissipationless quantum spin current at room temperature, Science 301, 1348 (2003).

[4] J. Sinova, D. Culcer, Q. Niu, N. A. Sinitsyn, T. Jungwirth, and A. H. MacDonald, Universal Intrinsic Spin Hall Effect, Phys. Rev. Lett. 92, 126603 (2004).

[5] See supporting online material.

[6] M. W. Wu, J. H. Jiang, and M. Q. Weng, Spin dynamics in semiconductors, Phys. Rep. 493, 61 (2010).

[7] T. Kimura, Y. Otani, T. Sato, S. Takahashi, and S. Maekawa, Room-temperature reversible spin Hall effect, Phys. Rev. Lett. 98, 156601 (2007).

[8] T. Seki, Y. Hasegawa, S. Mitani, S. Takahashi, H. Imamura, S. Maekawa, J. Nitta, and K. Takanashi, Giant spin Hall effect in perpendicularly spin-polarized FePt/Au devices, Nature Mater. 7, 125 (2008).

[9] I. Tamm, Über eine mögliche Art der Elektronenbindung an Kristalloberflächen, Physik. Z. Sowjetunion 1, 733 (1932).

[10] E. W. Plummer and W. Eberhardt, Angle-resolved photoemission as a tool for the study of surfaces, Adv. Chem. Phys. 49, 533 (1982).

[11] S. LaShell, B. A. McDougall, and E. Jensen, Spin splitting of an Au(111) surface state band observed with angle resolved photoelectron spectroscopy, Phys. Rev. Lett. 77, 3419 (1996); G. Nicolay, F. Reinert, S. Hüfner, P. Blaha, Spin-orbit splitting of the L-gap surface state on Au(111) and Ag(111), Phys. Rev. B 65, 033407 (2001); M. Hoesch, M. Muntwiler, V. N. Petrov, M. Hengsberger, L. Patthey, M. Shi, M. Falub, T. Greber, and J. Osterwalder, Spin structure of the Shockley surface state on Au(111), Phys. Rev. B 69, 241401(R) (2004).

[12] L. Petersen and P. Hedegård, A simple tight-binding model of spin-orbit splitting of sp-derived surface states, Surf. Science 459, 49 (2000).

[13] T. Hirahara, K. Miyamoto, I. Matsuda, T. Kadono, A. Kimura, T. Nagao, G. Bihlmayer, E. V. Chulkov, S. Qiao, K. Shimada, H. Namatame, M. Taniguchi, and S. Hasegawa, Direct observation of spin splitting in bismuth surface states, Phys. Rev. B 76, 153305 (2007).

[14] M. Hochstrasser, J.G. Tobin, E. Rotenberg, and S. D. Kevan, Spin-resolved photoemission of surface states of W(110)-(1×1)H, Phys. Rev. Lett. 89, 216802 (2002).

[15] E. Rotenberg, J. W. Chung, and S. D. Kevan, Spin-orbit coupling induced surface band splitting in Li/W(110) and Li/Mo(110), Phys. Rev. Lett. 82, 4066 (1999).

[16] A. M. Shikin, A. Varykhalov, G. V. Prudnikova, D. Usachov, V. K. Adamchuk, Y. Yamada, J. D. Riley, and O. Rader, Origin of spin-orbit splitting for monolayers of Au and Ag on W(110) and Mo(110), Phys. Rev. Lett. 100, 057601 (2008).

[17] A. Varykhalov, J. Sánchez-Barriga, A. M. Shikin, W. Gudat, W. Eberhardt, and O. Rader, Quantum cavity for spin due to spin-orbit interaction at a metal boundary, Phys. Rev. Lett. 101, 256601 (2008).

[18] J. H. Dil, F. Meier, J. Lobo-Checa, L. Patthey, G. Bihlmayer, and J. Osterwalder, Rashba-type spin-orbit splitting of quantum well states in ultrathin Pb films, Phys. Rev. Lett. 101, 266802 (2008).

[19] A. Varykhalov, J. Sánchez-Barriga, A. M. Shikin, C. Biswas, E. Vescovo, A. Rybkin, D. Marchenko, and O. Rader, Electronic and Magnetic Properties of Quasifree-standing Graphene on Ni, Phys. Rev. Lett. 101, 157601 (2008).

[20] Ch. S. Ast, J. Henk, A. Ernst, L. Moreschini, M. C. Falub, D. Pacilé, K. Kern and M. Grioni, Giant spin splitting through surface alloying, Phys. Rev. Lett. 98, 186807 (2007).

[21] A. T. N'Diaye, J. Coraux, T. N. Plasa, C. Busse, T. Michely, Structure of epitaxial graphene on Ir(111), New J. Phys. 10, 043033 (2008).

[22] J. F. van der Veen, F. J. Himpsel, and D. E. Eastman, Structure-dependent 4f-core-level binding-energies for surface atoms on Ir(111), Ir(100)-(5×1), and metastable Ir(100)-(1×1), Phys. Rev. Lett. 44, 189 (1980).

[23] M. Bianchi, D. Cassese, A. Cavallin, R. Comin, F. Orlando, L. Postregna, E. Golfetto, S. Lizzit and A. Baraldi, Surface core level shifts of clean and oxygen covered Ir(111), New J. Phys. 11, 063002 (2009).

[24] P. Lacovig, M. Pozzo, D. Alfé, P. Vilmercati, A. Baraldi, S. Lizzit, Growth of Dome-Shaped Carbon Nanoislands on Ir(111): The Intermediate between Carbidic Clusters and Quasi-Free-Standing Graphene, Phys. Rev. Lett. 103, 166101 (2009).

[25] J. F. van der Veen, F. J. Himpsel, and D. E. Eastman, Experimental energy dispersions for valence and conduction bands of iridium, Phys. Rev. B 22, 4226 (1980).

[26] I. Pletikosić, M. Kralj, D. Sokcević, R. Brako, P. Lazić, and P. Pervan, Photoemission and density functional theory study of Ir(111); energy band gap mapping, J. Phys.: Condens. Matter 22, 135006 (2010).

[27] I. Pletikosić, M. Kralj, P. Pervan, R. Brako, J. Coraux, A. T. NDiaye, C. Busse, T. Michely, Dirac Cones and Minigaps for Graphene on Ir(111), Phys. Rev. Lett. 102, 056808 (2009).

[28] G. Giovannetti, P. A. Khomyakov, G. Brocks, V. M. Karpan, J. van den Brink, and P. J. Kelly, Doping graphene with metal contacts, Phys. Rev. Lett. 101, 026803 (2008).

[29] C. L. Kane and E. J. Mele, Z_2 topological order and the quantum spin Hall effect, Phys. Rev. Lett. 95, 226801 (2005); B. A. Bernevig and S. C. Zhang, Quantum spin Hall effect, Phys. Rev. Lett. 96 106802 (2006); M. König *et al.*, Quantum spin hall insulator state in HgTe quantum wells, Science 318, 766 (2007); J. E. Moore and L. Balents, Topological invariants of time-reversal-invariant band structures, Phys. Rev. B 75, 121306 (2007); R. Roy, Topological phases and the quantum spin Hall effect in three dimensions, Phys. Rev. B 79, 195322 (2009); S. Murakami, Phase transition between the quantum spin Hall and insulator phases in 3D: emergence of a topological gapless phase, New J. Phys. 9, 356 (2007).

[30] Y. Xia, D. Qian, D. Hsieh, L. Wray, A. Pal, H. Lin, A. Bansil, D. Grauer, Y. S. Hor, R. J. Cava, and M. Z. Hasan, Observation of a large-gap topological-insulator class with a single Dirac cone on the surface, Nature Phys. 5, 398 (2009).

[31] D. Hsieh *et al.*, Observation of Unconventional Quantum Spin Textures in Topologically Ordered Materials, Science 323, 919 (2009).

[32] V. A. Mozhayskiy, A. Y. Varykhalov, A. G. Starodubov, A. M. Shikin, S. I. Fedoseenko, and V. K. Adamchuk, Formation of mono-atomic carbon layers on Ni(111) by means of organic-gas cracking and by thermal decomposition of fullerenes in thin film, Phys. Low-Dim. Struct., Issue 1-2, 105 (2003). See Supplementary Material for more recent references.

[33] Supplementary information for this paper is enclosed.

Supplementary information for

Topological surface state under graphene for two-dimensional spintronics in air

A. Varykhalov, D. Marchenko, M. R. Scholz, E. Rienks, T. K. Kim, and O. Rader

Methods

Experiments were conducted in ultrahigh vacuum better than 1×10^{-10} mbar. The clean Ir(111) surface was prepared by cycles of Ar^+ sputtering followed by annealing at 1600 K. The graphene layer was grown epitaxially by chemical vapour deposition of propene at 1150 K and a partial pressure of 3×10^{-8} mbar. Spin- and angle-resolved photoemission measurements were performed with electron analysers Scienta R8000 (setup ARPES 1^2) and SPECS PHOIBOS 150 using linearly polarized synchrotron radiation from the beamlines UE112-PGM1 and UE112-lowE-PGM2 at BESSY II. Spin resolution was done with a Rice University Mott polarimeter operated at 26 kV [34]. The setup is sensitive to the two spin quantization axes in the surface plane of the sample, and Fig. 3j-l shows the spin component tangential to the energy surfaces which are shown in Fig. 3e-h. Scanning tunneling microscopy (STM) images were acquired with an Omicron VT-STM at room temperature.

Sample characterization

Prior to the detailed investigation of bare Ir(111), its cleanliness was verified by observation of a sharp $p(1\times1)$ pattern in LEED (Fig. 1a) and by the absence of carbon-derived electronic states in valence-band photoemission. After covering the Ir with graphene, quality and completeness of the graphene layer were extensively tested. The samples have been characterized in situ with LEED (Fig. 1b) and in a separate setup with STM (Fig. S1a). The results of LEED and STM are in full agreement with previous reports [20].

The *in situ* characterization by ARPES showed typical features of the moiré pattern reported in the literature [27]: The Dirac cone is subject to lateral quantization by the moiré superlattice (Fig. S1b). Minigaps (dashes) appear where umklapp-induced replica bands (white arrows) intersect [27]. The characteristic trigonal symmetry of the Dirac cone as well as its two-dimensional replication within the surface Brillouin zone are well seen in constant binding energy surfaces (Fig. S1c).

Topological nontrivial character of the surface state - theoretical support

We present here strong indications for a topological nontrivial character of the investigated surface state. Fig. S2a shows the calculated band structure of Ir along [111] (Γ-Λ-L-direction) [35]. Unlike with noble metals, there is no band gap along [111] near E_F because the red and the blue band overlap energetically in some part of the Λ-direction. As the present surface state is situated between the red and the blue band, it is strictly speaking a surface resonance. The red bulk band is of Λ_6^3 symmetry (subscript for double-group, superscript for single-group notation) and extends up to E_F and above. The blue bulk band is a Λ_6^1 band with the noted energetical overlap with the Λ_6^3 band in the range around 1 eV binding energy. These bands have opposite parities at the L point, L_{6-}^1 and $L_{6+}^{2'}$, respectively. From the band structure it appears thus that the surface state couples at L bulk states of odd parity and even parity which renders it odd, rather similar to the situation after band inversion in HgTe quantum wells creating a topological state as well [36].

In Fig. S3a-b we show the criterion for topological protection of the surface state. Between two time-reversal invariant points of the surface Brillouin zone, i. e., here the two-dimensional $\overline{\Gamma}$ and $\overline{M}$ points, the topological surface state must cross only an odd number of times an arbitrary line between the upper and lower bulk bands. This criterion replaces that for topological insulators with an absolute band gap at E_F (Fig. S3a). Fig. S3b shows three different choices for such line proving that it cuts the surface state only an odd number of times.

Topological nontrivial character of the surface state - experimental support

Fig. 3a-c of the manuscript has shown that the surface state consists of entangled bands that cross at $k_{\|}$=0. This is very different from the finding of two parallel dispersions in Ref. 26. A possible reason could be a slight mis-

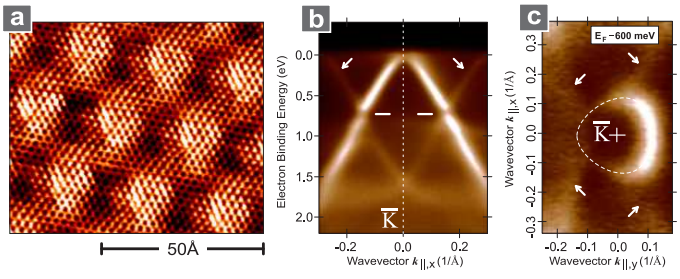

Figure S1. Effects of the moiré-type superstructure of graphene/Ir(111) in (**a**) STM and (**b,c**) ARPES.

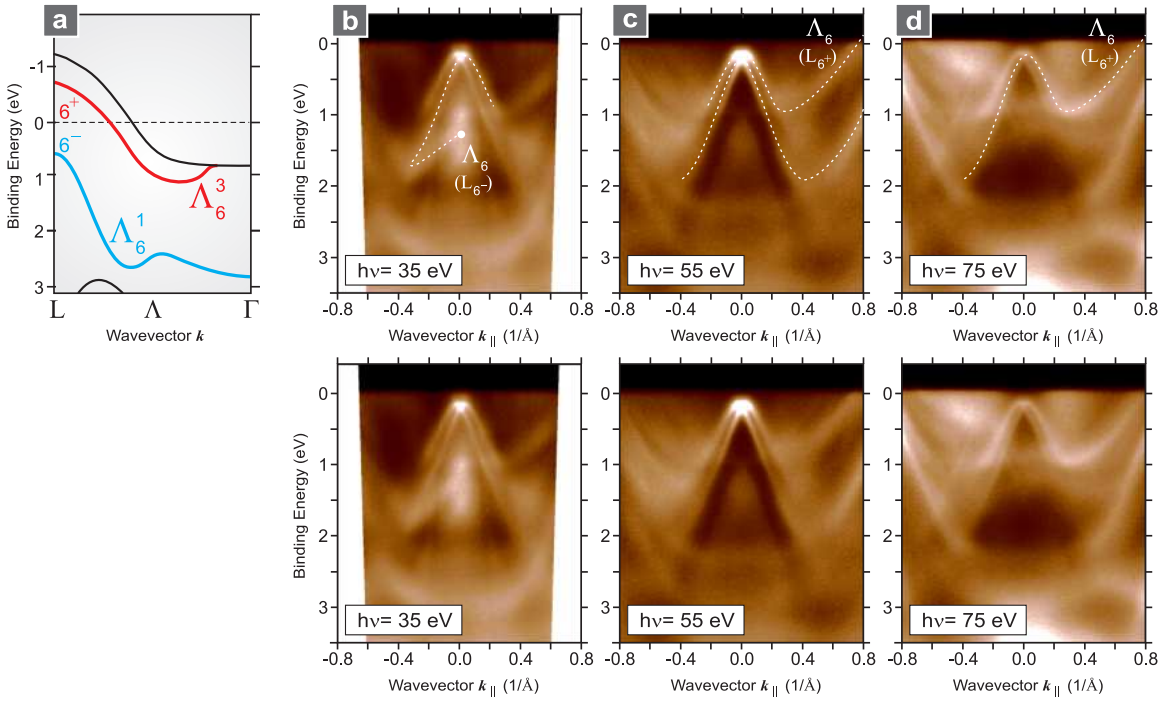

Figure S2. (**a**) Calculated Ir bulk bands along [111] [35]. The surface state is situated in between the red and the blue band. (**b-d**) Photon-energy and, hence, $\mathbf{k}_\perp$ dependence of the topological surface state and the adjacent bulk bands.

alignment away from $k_\parallel$=0 in Ref. 26 because this would automatically lead to the disappearance of the crossing point.

Fig. S2b-d [37] shows that the surface state does not change when the photon energy is varied from 35 eV over 55 eV to 75 eV which changes the electron wave vector component perpendicular to the surface, $\mathbf{k}_\perp$. This proves its two-dimensional character.

Other bands in Fig. S2b-d do, however, change strongly and are, therefore, derived from the three-dimensional bulk. In Fig. S2b we see that the inner cone of the surface state connects for negative $k_\parallel$ to a bulk band which reaches normal emission and thus the Γ-Λ-L line at 1.0-1.5 eV binding energy. From Fig. S2a we identify this bulk band as the lower Λ_6^1 band (blue) which connects to the L_{6-}^1 point of odd parity. Fig. S2c shows how at 55 eV the surface state connects for positive $k_\parallel$ to a bulk band which disperses upwards and crosses E_F. There are few bulk bands which cross E_F [35]. The lower Λ_6^1 band does not cross E_F but the upper Λ_6^3 band does so. So, even though the band in Fig. S2c is not sampled along the Λ line, it is most likely that it is connected to this band. Fig. S2c also shows how the surface state connects to the lower bulk band (blue) at this higher photon energy and different value of $\mathbf{k}_\perp$ dispersing differently with $\mathbf{k}_\parallel$. Finally, Fig. S2d shows in the same data set that the surface state connects with its outer cone (for positive $k_\parallel$) to the upper bulk band (red) and with its inner cone (for negative $k_\parallel$) to the lower bulk band (blue).

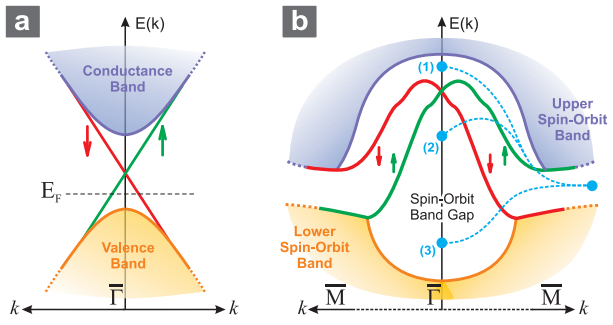

Figure S3. Comparison of (**a**) the topological insulator and (**b**) the present case of a topological metal. (1), (2), and (3) denote three different choices for connecting time-reversal invariant points $\overline{\Gamma}$ and $\overline{\mathrm{M}}$ between the confining bulk bands.

Fig. S3 shows the relation of the present topological surface state on a metal to that on a topological insulator with absolute band gap. The surface state on a topological metal has at first been noted for Sb(111) [31]. For the topological insulator, an odd number of crossings of the Fermi energy between two time-reversal invariant points of the surface Brillouin zone is the necessary criterion. This means for the topological metal that any line connecting two time-reversal invariant points, here $\overline{\Gamma}$ and $\overline{\mathrm{M}}$, inside of the gap between the upper and lower bulk band must be crossed an odd number of times. This is shown

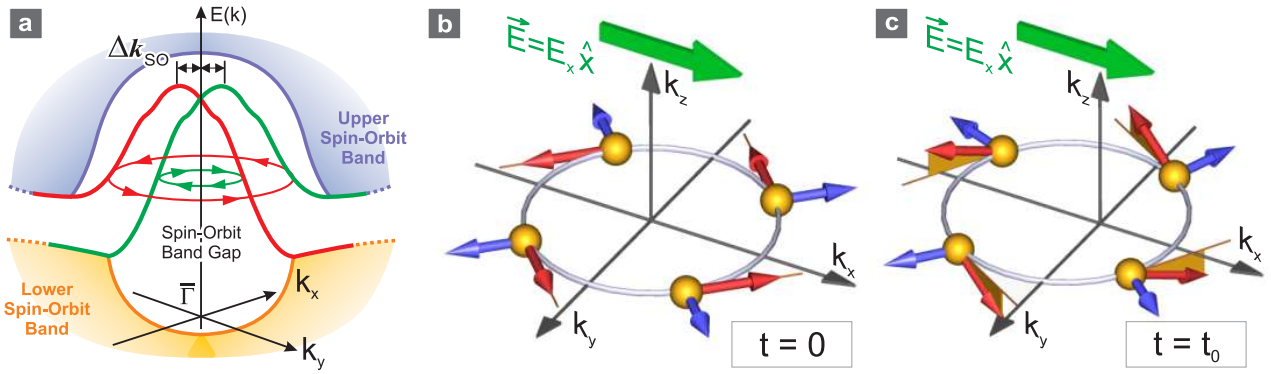

Figure S4. (**a**) Sketch of the present Rashba-split topological surface state. (**b**) Constant-energy surface with directions of momentum (blue) and spin (red). (**c**) An external electric field leads to a spin tilting and spin current in the perpendicular in-plane direction, according to Ref. [4].

for three examples (1) through (3) in Fig. S3b.

Principle of devices

The device for creation of a spin current from a Rashba-split electronic structure is based on the intrinsic spin Hall effect. It is different from the historically older extrinsic spin Hall effect which is due to scattering from impurities [38]. The generation of spin currents does not require the band gap of a semiconductor. The generation and, not less difficult, the measurement of spin currents has made impressive progress in recent years. Currently, the spin Hall effect and inverse spin Hall effect have evolved into the most important processes for generation and measurement, respectively. The spin Hall effect has been proven at first for semiconductors [39] and for a two-dimensional electron gas [40-42]. However, the size of the effect in metals is much larger. It was shown that in Pt it is by 4 orders of magnitude larger than in semiconductors [43], and an FePt/Au device increased the effect further by another factor of 10 [44].

Fig. S4b shows how a spin current is created by a charge current in a system with Rashba-type spin-orbit interaction. The figure shows a sketch of a Rashba-split system adopted to the present situation from Ref. [4]. Due to the Rashba effect the electron momentum (blue) is coupled to the spin (red). For the case of circular constant energy surfaces as seen in the experimental data in Fig. 3e-h, it is tangential to these constant energy surfaces and perpendicular to the momentum. Fig. S4b shows for $t=0$ the equilibrium situation when the external electric field is switched on. Fig. S4b shows further how the constant energy surface has shifted at t_0 along k_x by $\Delta k_x = \frac{eE_x t_0}{\hbar^2}$. The movement leads in the perpendicular direction k_y to a spin torque which tilts the spins up for $k_y > 0$ and down for $k_y < 0$. The contributions from the Fermi surface lead to a spin current in the y-direction.

The effect of the graphene formation lifts the top of the surface state from 340 meV to 190 meV (Fig. 3a,b), so the surface state does not yet cut the Fermi energy. Alloying with a heavy element to the left of Ir in the perodic system such as Os for amounts of the order of 20% should move the bulk band edges sufficiently up to make the surface state partially unoccupied.

The active element of a potential device is the surface of Ir(111) which can be grown as a thin film. The role of the graphene is to protect this surface against ambient atmosphere. This is realistic as we have shown that the presence of the graphene leaves the Rashba splitting of the surface state unaffected and this does not change even after exposure to atmospheric pressure.

Stability of graphene and graphene on metals to atmosphere

Graphene is stable at atmospheric pressure which is apparent from most experiments on exfoliated graphene flakes which are done under ambient conditions. If graphene would not be stable enough to protect the Ir surface against reactions with, e. g., oxygen, this would ultimately change the bulk electronic structure of the Ir and also remove the surface state. In this sense, the stability and protection of graphene on transition metal surfaces is a prerequisite for the present work. While graphene/Ir has not yet been studied in this respect, other transition metals have. We have shown early on that exposure of graphene/Ni(111) does not lead to oxidation of the Ni [45,46]. The same system has been exposed to oxygen at 6×10^{-6} mbar for 30 min [47], graphene/Fe/Ni(111) to similar conditions [48]. The system graphene/Ru(0001) has been exposed to oxygen partial pressure [49,50] and to atmosphere [50]. Surface electronic features of the transition metals have not been studied up to now.

References

[34] G. C. Burnett, T. J. Monroe, and F. B. Dunning, High-efficiency retarding-potential Mott polarization analyzer, Rev. Sci. Instrum. 65, 1893 (1994).

[35] J. Noffke and L. Fritsche, Band structure calculation and photoemission analysis of iridium, J. Phys. F.: Met. Phys. 12, 921 (1982).

[36] B. A. Bernevig, T. L. Hughes, and S.-C. Zhang, Quantum Spin Hall Effect and Topological Phase Transition in HgTe Quantum Wells, Science 314, 1757 (2006).

[37] J. Sánchez-Barriga, A. Varykhalov et al. (unpublished)

[38] J. E. Hirsch, Spin Hall effect, Phys. Rev. Lett. 83, 1834 (1999).

[39] Y. K. Kato, R. S. Myers, A. C. Gossard, and D. D. Awschalom, Observation of the spin hall effect in semiconductors, Science 306, 1910 (2004).

[40] J. Wunderlich, B. Kaestner, J. Sinova, and T. Jungwirth, Experimental observation of the spin-Hall effect in a two-dimensional spin-orbit coupled semiconductor system, Phys. Rev. Lett. 94, 047204 (2005).

[41] S. O. Valenzuela and M. Tinkham, Direct electronic measurement of the spin Hall effect, Nature 442, 176 (2006).

[42] E. Saitoh, M. Ueda, H. Miyajima, and G. Tatara, Conversion of spin current into charge current at room temperature: Inverse spin-Hall effect, Appl. Phys. Lett. 88, 182509 (2006).

[43] T. Kimura, Y. Otani, T. Sato, S. Takahashi, and S. Maekawa, Room-temperature reversible spin Hall effect, Phys. Rev. Lett. 98, 156601 (2007).

[44] T. Seki, Y. Hasegawa, S. Mitani, S. Takahashi, H. Imamura, S. Maekawa, J. Nitta, and K. Takanashi, Giant spin Hall effect in perpendicularly spin-polarized FePt/Au devices, Nature Mater. 7, 125 (2008).

[45] V. A. Mozhayskiy, A. Y. Varykhalov, A. G. Starodubov, A. M. Shikin, S. I. Fedoseenko, and V. K. Adamchuk, Formation of mono-atomic carbon layers on Ni(111) by means of organic-gas cracking and by thermal decomposition of fullerenes in thin film, Phys. Low-Dim. Struct., Issue 1-2, 105 (2003).

[46] V. A. Mozhayskiy, A. Y. Varykhalov, A. G. Starodubov, A. M. Shikin, S. I. Fedoseenko, and V. K. Adamchuk, Two alternative ways for formation of mono-atomic carbon layer on Ni(111): Organic-gas cracking and thermal decomposition of fullerenes in thin film, Fullerenes, Nanotubes and Carbon Nanostructures 12, 385 (2004).

[47] Y. S. Dedkov, M. Fonin, and C. Laubschat, A possible source of spin-polarized electrons: The inert graphene/Ni(111) system, Appl. Phys. Lett. 92, 052506 (2008).

[48] Y. S. Dedkov, M. Fonin, U. Rüdiger, and C. Laubschat, Graphene-protected iron layer on Ni(111), Appl. Phys. Lett., Appl. Phys. Lett. 93, 022509 (2008).

[49] H. Zhang, Q. Fu, Y. Cui, D. Tan, and X. Bao, Growth Mechanism of Graphene on Ru(0001) and O2 Adsorption on the Graphene/Ru(0001) Surface, J. Phys. Chem. C 113, 8296 (2009).

[50] B. Borca, F. Calleja, J. J. Hinarejos, A. L. Vázquez de Parga, and R. Miranda, Reactivity of periodically rippled graphene grown on Ru(0001), J. Phys.: Condens. Matter 21, 134002 (2009).